AMS Home   Journals Home   Journal Archive   Subscribe   For Authors   Help   Advanced Search   [Search] [Go]

Full Text View

Modeling the Wind-Driven Variability of the South Indian Ocean

R. P. Matano

College of Oceanic and Atmospheric Sciences, Oregon State University, Corvallis, Oregon

C. G. Simionato and P. T. Strub

CIMA-CONICET, Universidad Nacional de Buenos Aires, Buenos Aires, Argentina, and College of Oceanic and Atmospheric Sciences, Oregon State University, Corvallis, Oregon

ABSTRACT

This article describes the results of numerical experiments carried out with a general circulation ocean model to investigate the effect of the seasonal cycle of the wind forcing on the Agulhas transport. Two cases are described. The first was initialized with temperature and salinity values obtained by horizontally averaging Levitus climatology. The second experiment was designed to isolate the spatial and temporal structure of the barotropic mode. The model, therefore, was initialized with constant values of temperature and salinity. Both experiments were started from rest, forced at their surface with Hellerman and Rosenstein wind stress climatology, and spun up until dynamical equilibrium. According to the experiments there are two distinct modes of variability in the south Indian Ocean. These modes appear to be separated by the topographic ridges that run south of Madagascar. On the western side of the basin there is a dominant mode with a maximum during spring–summer and a minimum during fall–winter. East of Madagascar there is a marked decrease of the circulation in fall and relative maximums during late summer and late winter. The midlatitude time variability, east of 45°E, appears to be dominated by advection and wave propagation. West of 45°E there is dominance by local wind forcing. A comparison between baroclinic and barotropic experiments indicates that although their annual mean structure is markedly different, their monthly anomalies, south of 30°S, are quite similar. This result, which agrees with previous theoretical and experimental studies, indicates that the seasonal adjustment in the south Indian Ocean is mostly accomplished by the westward propagation of barotropic planetary waves. This propagation is inhibited by the bottom topography of the Madagascar Ridge and Southwest Indian Ridge (~ 45°E). These topographic features appear to isolate the Agulhas Current in the western region from the large-scale gyre farther east at seasonal timescales.

Options:
- Create Reference
- Email this Article
- Add to MyArchive
- Search AMS Glossary

Search CrossRef for:
- Articles Citing This Article

Search Google Scholar for:
- R. P. Matano
- C. G. Simionato
- P. T. Strub

1. Introduction and background

The upper circulation of the south Indian Ocean is characterized by an anticyclonic wind-driven gyre. It is limited to the north by the South Equatorial Current, to the south by the subtropical convergence, and closed to the west by the poleward flow of the Agulhas Current, the major western boundary current of the Southern Hemisphere. According to existing theories of the global thermohaline circulation, the south Indian Ocean links both the deep and upper circulation of the Atlantic and Pacific oceans (Gordon 1986). In the upper ocean this link is accomplished by the intermittent intrusion, into the southeast Atlantic, of warm and salty waters spawned from the retroflection of the Agulhas Current. The Agulhas Current flows southwestward along the eastern coast of southern Africa and separates from the coast near the southern tip of the continental slope. After separation it executes an abrupt anticyclonic loop, called the Agulhas Retroflection, and turns back into the Indian Ocean as an eastward flowing jet, known as the Agulhas Return Current. This current is characterized by the presence of large-scale meanders that have been related to topographic features such as the Agulhas Plateau and the Mozambique Ridge extension (Harris 1970).

The dynamics of the Agulhas Current and the causes of its retroflection have been discussed by previous authors. De Ruijter and Boudra (1985), Boudra and Chassignet (1988), and Chassignet and Boudra (1988) used primitive equation models in highly idealized, flat-bottomed basins. According to these studies the retroflection results from a balance between viscosity and inertia in a fluid moving across latitudinal lines. Ou and de Ruijter (1986) used an analytical model to investigate the effect of coastline curvature on the separation of the Agulhas Current from the coast. They showed that a coastline with a curvature like the African coast reinforces the gradient of planetary vorticity and reduces the centrifugal forces. Both effects lead to a premature separation from the coast. Lutjeharms and van Ballegooyen (1984) and Matano (1996) used semianalytical and numerical models to investigate the effect of bottom topography on the Agulhas Retroflection. They concluded that for realistic basin configurations the retroflection was the result of an inertially driven jet flowing over the shallow depths of the Agulhas Plateau.

The water characteristics of the Agulhas Current are dominated by contributions of tropical surface water, south Indian subtropical water, and tropical thermocline water (Lutjeharms and Ansorge 1999, manuscript submitted to *J. Phys. Oceanogr.*). Tropical surface waters, characterized by a salinity minimum, are derived from the South Equatorial Current through the Mozambique Current. The more saline subtropical and thermocline waters are drawn from the eastern gyre and from an intense inertial recirculation cell. Stramma and Lutjeharms (1997) calculated the transport field of the South Indian Ocean using historical hydrographic data and estimated that of the 65 Sv (Sv $\equiv 10^6$ m^3 s^{-1}) that constitutes the upstream Agulhas transport, 35 Sv are related to inertial recirculation, 25 Sv comes from east of Madagascar, and about 5 Sv flow through the Mozambique Channel. In spite of the fact that the Sverdrup balance indicates that the mass transport of the Agulhas Current should be 20 Sv higher during the Southern Hemisphere winter than during its summer (Hellerman and Rosenstein 1983), there are conflicting opinions in the literature about seasonal variations of the Agulhas transport. Pearce and Gründlingh (1982) used historic data to revisit previous transport estimates and concluded that there is no significant annual variation of the mean flow intensity. Seasonal changes in the Agulhas transport have been mostly surmised from satellite observations. Altimeter data and infrared imagery shows annual changes in rms variability of the sea surface elevation and temperature fields that have been related to zonal displacements of the retroflection region (Zlotnicki et al. 1989; Quartly and Srokosz 1993; Lutjeharms and van Ballegooyen 1988). Previous authors speculated that seasonal variations of the Agulhas transport might cause zonal displacements of the retroflection region and affect the rate of eddy formation.

The purpose of this article is to put forward a hypothesis that might explain the apparent discrepancy between in situ measurements, which have been unable to identify seasonal variations of the Agulhas transport, and satellite studies, which have described seasonal changes of the current's transport in the retroflection region. In order to introduce this hypothesis it should be noted that each type of observation usually refers to different portions of the Agulhas Current. Hydrographic observations, on the one hand, have been mostly collected in the portion of the current that flows parallel to the African continent. Remote observations, on the other hand, have been focused in the region south of the continent, that is, after the Agulhas Current leaves the continental slope and flows into the open ocean. The hypothesis to be presented is that these two regions have different dynamical characteristics that explain the seemingly contradictory observations. It will be argued that the lack of seasonal variations, reported in the northern portion of the flow, results from topographic effects that inhibit the westward propagation of the wind-driven signal. As the current leaves the coast however, it spreads over a wider region (the Agulhas Retroflection region), where strong wind anomalies influence the local circulation. To sustain this hypothesis we will discuss results of numerical experiments conducted with an ocean general circulation model.

This article has been organized as follows: after this introduction, section 2 offers a brief description of the numerical model used in these experiments and a discussion of its setup; section 3 describes the numerical experiments; and section 4 summarizes and discusses the results.

2. Model description

The model utilized in this study is the multilevel numerical model described by Bryan (1969) and implemented by Cox (1984). Its domain extends from 55° to 20°S and from 0° to 120°E. Bottom topography and coastlines are realistic with the exception of the inclusion of solid walls at open boundaries. Near these artificial boundaries we included regions of increased viscosity to avoid spurious reflections. The model has a horizontal resolution of 1° and 15 vertical levels. The focus of the simulations will be on the large-scale ocean adjustment. For the periods of interest to this study these are mostly barotropic processes, with spatial scales of the order of a thousand kilometers (the external Rossby radius), which are well represented in our model.

The bottom topography of the south Indian Ocean is characterized by a complex series of ridges and plateaus that subdivide the basin. The region covered in this study is shown in Fig. 1 ⌖. The western portion of the basin is partially isolated from the rest of the ocean by the Madagascar Ridge and the Southwest Indian Ridge, which run from approximately 30° to 48°S between 45° and 60°E. South of Africa, the most prominent feature is the Agulhas Plateau (40°S, 26°E), whose relatively shallow depths have been related to the retroflection of the Agulhas Current (Matano 1996). In what follows the term Agulhas Retroflection region (ARR) will refer to the area located between 35° and 45°S, 10° and 30°E. East of Madagascar the basin is further subdivided by the meridionally oriented Ninetyeast Ridge, at approximately 88°E, and the Southeast Indian Ridge, which runs from the northern boundary and 65°E to the southeast corner of the domain. The south-central portion of the basin is interrupted by the Kergulean Plateau, which runs south of 45°S between 60° and 80°E.

Two experiments will be discussed. The first one was initialized with temperature and salinity values obtained by horizontally averaging Levitus climatology. In this experiment the oceanic adjustment to the changing wind forcing consisted of barotropic and baroclinic motions. The second experiment was designed to isolate the spatial and temporal structure of the barotropic mode. The model, therefore, was initialized with constant values of temperature and salinity ($T = 10°C$; $S = 35$ psu). Both experiments were started from rest and forced with annual-mean average winds (Hellerman and Rosenstein 1983) until dynamical equilibrium. After this spinup time, 100 yr for the baroclinic experiment and 10 yr for the barotropic one, monthly wind anomalies were included and the experiments were run for an additional 10-yr period. The duration of the numerical experiments was chosen as a compromise between the timescales dictated by the propagation of Rossby waves and that related to diffusion process. For the baroclinic experiments the wave timescale is of the order of decades, while for the barotropic ones it is of the order of weeks (depending on the latitude). Vertical diffusion has a timescale of the order of centuries.

As a characterization of the wind stress forcing, Fig. 2 ⌖ shows the zonally averaged wind stress curl. At 30°S the wind curl has a minimum during February (summer) and a maximum between May and June. At 40°S there is a minimum in April and a maximum between August and September. The main difference between wind variations at these latitudes is a three-month shift of the peaks.

3. Experimental results

After the two experiments reached dynamical equilibrium we calculated mean values and monthly anomalies of the prognostic variables. The discussion of these results has been divided in four sections. Section 3a presents the results of the baroclinic experiments. Section 3b discusses the barotropic experiments and compares these results with the climatological wind stress patterns. Section 3c discusses the results of one experiment conducted in an extended basin to check the effects of lateral boundary conditions on the simulations. Section 3d compares the numerical results with observations and other numerical simulations.

a. The baroclinic experiment

The annual mean streamfunction distribution for the baroclinic experiment is shown in Fig. 3 ⌖. The circulation consists of an anticyclonic cell with a western boundary current, the Agulhas Current, flowing poleward along the eastern coast of Africa. The current has a maximum mass transport of approximately 50 Sv. After reaching the tip of South Africa, nearly 65% of the incoming flow retroflects while the remainder enters the southeast Atlantic. In the present simulations the retroflection is related to bottom topography, inertia, and viscous effects. The portion of the flow that continues into the South Atlantic reaches the solid western boundary, where it generates an artificial western boundary current that flows poleward and returns eastward. This artificial western boundary current is a byproduct of the nonflux conditions imposed at 0°. In a more realistic setting the incoming Agulhas flow would be entrained into the subtropical gyre and returned to the Indian Ocean by the eastward flow of the South Atlantic Current. Two precautions were taken to ensure that the boundary conditions at 0° do not affect the simulated wind driven variability in the south Indian Ocean: 1) a region of increased viscosity was added near the western boundary to prevent the eastward propagation of spurious reflections and 2) all the experiments were repeated in an extended domain that included the South Atlantic basin as well. A brief summary and discussion of these experiments are presented in section 3c.

The baroclinic response of the ocean to the seasonal wind stress forcing is illustrated by the time evolution of the streamfunction along 30° and 40°S (Fig. 4 ⊙). At 30°S the streamfunction fields near the African coast (~ 33°E) varies from 20 Sv (April–August) to 23 Sv (September–March). Farther east, over the Madagascar Ridge, the streamfunction fields have a transport minima in April (~ 20 Sv) and a maximum during August. The crowding of isolines over the Madagascar Ridge (~ 45°E) indicates that the largest seasonal changes occur east of 45°E with a range of approximately 20 Sv, while variations in the region occupied by the Agulhas Current have a maximum amplitude less than 5 Sv. In a more realistic setting these relatively small variations can be easily masked by higher-frequency perturbations, for example, they form instabilities of the mean flow or short-term wind variations. The small amplitude of the seasonal changes in the Agulhas transport is related to the isolating effect of the Madagascar Ridge, which prevents the westward transmission of wind energy from the open ocean to the western boundary. Thus, seasonal changes in the wind-forced transport, at 30°S, are more likely to be observed over the Madagascar Ridge than near the African continent. The transect at 40°S is located south of the African continent (Fig. 1 ⊙), and therefore covers the ARR. The variability in this transect is characterized by two distinct modes, roughly separated by the Atlantic–Indian Ridge. East of the ridge the streamfunction follows the time evolution of the zonally averaged wind stress curl. There is a strong decrease of the circulation during April and a maximum during August. To the west of the Madagascar Ridge, and over the ARR (approximately between 20° and 30°E), there is a strengthening of the circulation from spring to summer (October–March) and a weakening during fall (April–May).

A comparison between oceanic and atmospheric variability (Fig. 2 ⊙ and Fig. 4 ⊙) shows that while some regions of the ocean appear to follow a time-dependent Sverdrup balance, others do not. As an example, Fig. 5 ⊙ shows the time evolution of the zonally averaged wind stress curl at 30° and 40°S superimposed to transport anomalies at 57°E. At 30°S transport changes of the East Madagascar Current appears to follow atmospheric anomalies with a phase lag between 1 and 2 months. April's transport decrease, for example, relates to a dip of the zonally averaged wind stress curl that peaked in March, while August's transport maximum trails a similar intensification of the wind stress curl during the austral winter. At 40°S the correlation between oceanic and atmospheric variables is not obvious. The marked decrease observed during April appears to be mostly related to the circulation minimum at 30°S and not to wind variations. In this case north–south advection associated with the meridional flow of the East Madagascar Current transmits wind information from low to high latitudes that dominate the regional oceanic variability. In the following section we will show that because of the predominant barotropic structure of the perturbations oceanic anomalies not only depend on the wind stress curl, but also on the details of bottom topography.

To help the visualization of the oceanic variability we calculated streamfunction anomalies by subtracting the annual mean from the monthly values. Figure 6 ⊙ shows the spatial distribution of the streamfunction anomalies for the months of February (summer), May (fall), August (winter), and November (spring). In these panels positive/negative values mean a strengthening/weakening of the anticyclonic circulation cell (Fig. 3 ⊙). The geographical distribution of major anomaly patterns roughly corresponds with the bottom topography of the basin. There is a generalized weakening of the circulation during May and a well-defined intensification, between 45° and 75°E, during August. During the month of February there is an intensification of the anticyclonic circulation over the ARR and a weakening of the circulation in the region close to Madagascar. The upper-ocean circulation in this region is dominated by the poleward flow of the East Madagascar Current. According to historic data the East Madagascar Current is one of the main tributaries to the Agulhas transport (Lutjeharms 1996). After reaching the southernmost point of the island, a portion of the East Madagascar Current retroflects while the remainder continues westward. Hydrographic observations indicate that, although at depth there is a continuous inflow of East Madagascar waters into the Agulhas Current, the upper layers, mostly dominated by the East Madagascar Retroflection, connect only sporadically (Lutjeharms 1996). It is possible that a decrease of the East Madagascar transport during the summer months might lead to a weakening of its retroflection and increase the amount of surface waters attributed to the Agulhas Current. This inflow increase, plus the augmented circulation related to local winds (see Figs. 4 ⊙ and 6 ⊙), could produce the observed strengthening of the Agulhas Retroflection during the summer months that has been surmised from satellite observations (e.g., Quartly and Srokosz 1993).

Perhaps the most distinctive characteristic of Fig. 6 ⊙ is a general separation of anomaly patterns on either side of 50°E. The bottom topography of this region is characterized by the Madagascar Ridge and the Southwest Indian Ridge (Fig. 1 ⊙). According to theory and numerical experiments their relatively shallow depths can prevent the westward propagation of the barotropic Rossby waves that transmit the wind changes to the ocean's interior (Matano 1995). As a result, there is an accumulation of wind-driven energy over the ridges and a decoupling of variabilities on either side. Both effects can easily be appreciated in Figs. 4 ⊙ and 6 ⊙. The topographic decoupling is particularly evident in the phase lags between the anomalies over the Agulhas Retroflection region and those on the eastern portion of the basin. Sometimes these anomalies are completely out of phase, for example, in August when there is a strengthening in the circulation east of Madagascar and a weakening to the west of it. As we shall show, the anomaly patches that extend over the ARR are not the result of westward energy propagation but rather of the interaction between local wind forcing and bottom topography.

b. The barotropic experiment

The annual mean distribution of the streamfunction for the barotropic experiment is shown in Fig. 7 ⊙. The differences with the baroclinic experiment (Fig. 3 ⊙) are notable. The most striking feature of the barotropic calculation is the absence

of a well-defined Agulhas Current along the eastern coast of Africa. The average barotropic circulation consists of a zonally constrained, anticyclonic cell flanked to the west by two meridional jets flowing along the eastern slopes of the Southwest Indian Ridge and the Madagascar Ridge (Fig. 1 ⊙). Because of their depth-independent structure, the planetary waves that distribute the wind energy along the basin are highly sensitive to the bottom configuration (Rhines 1969; Matano 1995). A change of bottom depth, such as those observed near the Madagascar Ridge or the Southwest Indian Ridge, is an effective barrier against the westward propagation of the wave energy, therefore impeding the formation of a well-defined structure for the western boundary current.

The differences between Figs. 3 ⊙ and 7 ⊙ reflect the role of density stratification on the oceanic adjustment. In spite of the differences that may exist between *mean* barotropic and baroclinic circulations, it has long been argued that the adjustment of a baroclinic ocean to seasonal changes of the wind forcing is quite similar to that of a barotropic one (Gill and Niiler 1973; Anderson and Corry 1985; Willebrand et al. 1980). The barotropic adjustment is then followed by a baroclinic response in the form of a westward propagating Rossby wave. In the wake of this wave, the flow in the lower layer vanishes and the circulation becomes independent of bottom topography. At midlatitudes, however, the baroclinic propagation is so slow that even at seasonal timescales the response in the interior of the ocean is still described primarily by the barotropic Sverdrup relation. Theory therefore indicates that, although the mean circulation of barotropic and baroclinic experiments can be substantially different, their month-to-month anomalies are not. Figure 8 ⊙ shows the streamfunction anomalies for the barotropic experiment. Their similarities to Fig. 6 ⊙ corroborate the dominant role played by the barotropic mode in the seasonal adjustment of the south Indian Ocean. Major discrepancies are mostly confined to latitudes north of 30°S, where baroclinic waves have higher phase speeds and therefore contribute to the oceanic adjustment.

To gain more insight into the wind-driven variability it is useful to compare the monthly variability patterns of the ocean circulation with those of the wind stress curl (Fig. 9 ⊙). Since the barotropic adjustment is very fast (less than a week), we expect a reasonable correspondence between them. An overall comparison between Figs. 8 ⊙ and 9 ⊙ shows that this is indeed the case. During the month of February the decrease of the anticyclonic oceanic circulation north of 40°S and east of 50°E corresponds to a weakening of the atmospheric forcing (negative wind stress curl anomalies). South of 40°S these patterns reverse. A direct balance between the local wind stress curl and ocean currents, in contrast to a zonally integrated time-dependent Sverdrup balance, seems to dominate the dynamics of several regions of the ocean. Notice, for example, the correspondence between streamfunction and wind stress anomalies at 45°S, 80°E or along 60°E in Figs. 8a ⊙ and 9a ⊙. As we shall show, the anomalies on the ARR are also the result of local wind forcing instead of remote propagation. During the month of May, Fig. 9b ⊙ indicates a generalized weakening of the atmospheric circulation over the subtropical gyre, except in the region between 35° and 20°S, 35° and 70°E where there is an increase of the anticyclonic wind stress forcing that reflects in a weak acceleration of the oceanic gyre (Fig. 8b ⊙). During August the increased atmospheric circulation over the subtropical gyre (45° to 20°S, 30° to 120°E) results in an acceleration of the subgyre bounded by Madagascar to the west and the 80° meridian to the east (Fig. 8c ⊙). During the month of November, Fig. 9d ⊙ indicates that the atmospheric circulation has no significant departures from the annual mean except in the ARR. In correspondence with the atmospheric circulation, the oceanic anomalies depicted in Fig. 8d ⊙ shows little variation.

In the ARR, the anomaly patterns during August and November offer a clear example of the effect of local forcing on the circulation variability. During August the circulation in the ARR decreases, in spite of the fact that it increases in the eastern portion of the gyre. Likewise, the clear intensification of the circulation in the ARR during November appears unrelated to the weak changes occurring in the rest of the subtropical gyre. The observed decoupling at either side of the Madagascar Ridge indicates that although the mean circulation in the ARR is determined by the large-scale structure of the wind stress forcing, its monthly anomalies are mostly related to the curl of the local winds. This local balance is more evident in Fig. 10 ⊙, which shows the time series of the wind stress curl, averaged in the area between 35° and 45°S, 10° and 30°E, and the Agulhas transport at 40°S, 20°E. Local wind forcing causes an intensification of the ARR circulation during summer and a weakening during winter. A question put forward by one of the reviewers is whether a 5–6 Sv variation of the ARR circulation is significant. From a modeling point of view the observed signal is robust in the sense that it has a scale large enough to be well resolved by the model and strong enough to survive horizontal diffusion. Whether it is also significant cannot be determined from this study because of our lack of eddy resolution. Satellite observations however, which smoothed the high-frequency variability that characterize this region, indicate that the ARR is prone to seasonal variations, which are in agreement with the model predictions (e.g., Quartly and Srokosz 1993; Ffield et al. 1997).

It is interesting to note that although the phase of the transport's change in Fig. 10 ⊙ follows the time evolution of the wind stress curl, the largest anomalies occur over the Agulhas Plateau (Fig. 6 ⊙ and 8 ⊙). This indicates that, in the present simulations, the ARR variability is determined by the effect of regional winds blowing over relatively shallow depths. Since the forcing term in the barotropic vorticity equation is proportional to curl(τ/H) (e.g., Anderson and Corry 1985), changes in the transport of a western boundary current depend not only on the wind stress curl but also on its local component. Wind stress forcing along topographic contours can generate transport variations, even if the wind has no curl. To estimate the effect of local winds on the ARR variability we split the forcing term curl(τ/H) into its two components (one proportional to the curl of the wind stress, the other to the gradient of bottom topography). Figure 11 ⊙ shows the different terms averaged in the area between 35° and 45°S, 10° and 30°E. This figure indicates that, although the wind stress curl is the dominant forcing mechanism, the contribution of local winds blowing over varying depths became

particularly important during the fall and winter seasons. The local winds effects tend to balance those of the wind curl, therefore decreasing the amplitude of the resulting oceanic anomalies.

Past studies using satellite information have already suggested that the flow in the region of the Agulhas Retroflection may have seasonal variations. Zlotnicki et al. (1989) used 17 months of Geosat altimeter data to calculate the mean mesoscale variability in the region that extends from 35° to 41°S and 10° to 35°S. Their results showed a mean variability that decreased between July and September 1987 and increased from November to December 1986. These cycles coincide with the strengthening (during summer) and weakening (during winter) of the mean circulation predicted by the present simulations. Quartly and Srokosz (1996) analyzed the seasonal variability of the Agulhas Retroflection region using Geosat and AVHRR data and the output from the Fine Resolution Antarctic Model. Their examination of seasonal values showed the greatest variations to be in December–February (summer) and June–August (winter), the maximum being farther south during the austral summer and farther west during the winter. It was argued that these changes were more related to a displacement of the high variability region rather than to an increase or decrease in variability at a particular location. To explain these changes the authors speculated that a low Agulhas transport (during winter) may allow the current to follow the coast and penetrate farther westward. An increased transport during summer, as suggested by our numerical experiments, may force an earlier separation of the current from the coast and a southerly retroflection.

c. The extended domain experiments

One of the earlier concerns about the modeling strategy was the possibility that the nonflux conditions imposed at 0° might cause reflections that contaminate the interior solution. To avoid such possibility we added a sponge layer (a region of increased viscosity) near the western boundary. Such a device has been used with satisfactory results in previous experiments (e.g., Matano 1996). Nevertheless, in order to ensure the quality of the results we repeated all the experiments in an extended domain that included the South Atlantic basin as well. To avoid any eastward propagation, the wind forcing was tapered in the South Atlantic basin and the horizontal viscosity of the model was increased near the South American coast. The spinup of these experiments was identical to the cases just discussed. Figure 12 ⬤═ shows results obtained for the baroclinic experiment. The upper panel shows the streamfunction distribution after 100 yr of model integration using as forcing the annually averaged climatological wind stress (Hellerman and Rosenstein 1983). The most important difference with the previous case is the penetration of the Agulhas overflow into the South Atlantic basin and the formation of a pseudo Brazil Current against the eastern margin of South America; otherwise the streamfunction distribution is almost identical to the case described in section 3a. The similitude between the experiments in the two basins is more evident in the lower panel of Fig. 12 ⬤═, which shows the time evolution of the streamfunction at 40°S. A comparison with Fig. 4b ⬤═ shows no major disagreements east of 5°W. Since similar results were obtained for the barotropic case it was concluded that the boundary condition imposed at 0° did not affect the mean circulation patterns nor their variability.

d. Comparison with observations and other numerical simulations

Observations indicate that the bottom topography of the Indian Ocean not only affects its wind driven variability, as reported in this article, but also its mean circulation. In a recent description of the south Indian Ocean circulation, Stramma and Lutjeharms (1997) noted a remarkable asymmetry between the eastern and western portions of the subtropical gyre. West of 50°E the circulation is characterized by a strong recirculation cell, which accounts for approximately half of the Agulhas transport. Although in other western boundary currents (e.g., the Gulf Stream) recirculation cells have been associated with inertial effects, in the Agulhas case the recirculation seems to be driven by interactions between the Madagascar Ridge and the Agulhas Return Current. Topography also appears to affect the mean circulation patterns farther east. Stramma and Lutjeharms (1997) and Lutjeharms and Ansorge (1999, manuscript submitted to *J. Phys. Oceanogr.*) reported that, of the 60 Sv carried eastward by the Agulhas Return Current, 20 Sv recirculates between 40° and 50°E (the approximate location of the Madagascar Ridge), another 20 Sv between 60° and 70°E (Southwest Indian Ridge), while the remaining 20 Sv splits up into 10 Sv returning west at approximately 90°E (Ninetyeast Ridge) and 10 Sv flowing northward near Australia.

Ffield et al. (1997) used hydrographic data collected from two cruises and altimeter information from the TOPEX/Poseidon mission to estimate the seasonal changes in the south Indian Ocean subtropical gyre. Agulhas transports, calculated from hydrographic data along 32°E for the months of March and June of 1995, showed no significant seasonal variations. The ambiguity of these baroclinic estimates (which were both very close to the historical mean) is in agreement with our numerical prediction that at 30°S the seasonal cycle of the Agulhas Current should be very small (e.g., Fig. 4 ⬤═). Ffield et al. also used altimeter data to calculate upper-ocean geostrophic transports of the Agulhas Current, the southwest subgyre, and the Indian gyre. According to their estimates, the circulation has a maximum during March and September and is at its weakest during June and December. These seasonal variations closely follow those calculated from the Sverdrup relation. In spite of differences between the wind conditions for the TOPEX/Poseidon period (1992–96) and Hellerman and Rosenstein's (1983) climatology, the estimates of Ffield et al. for the interior gyre evolution are in general agreement with our results. The most conspicuous difference between the Ffield et al. calculations and our own concerns the annual variations of the Agulhas Current. According to their altimeter estimates, the Agulhas transport (defined by differences in sea surface height between 31.1°S, 30.4°E and 32.2°S, 32.5°E) closely follows the evolution of the interior gyre and basin-scale

winds with an amplitude of approximately 15 Sv. A possible explanation for this discrepancy is that during the period considered by Ffield et al. the wind stress of the southwestern subgyre had a similar time evolution as that of the whole basin. This indeed seems the case, as their estimate of the time evolution of the circulation in the southwestern Indian subgyre closely follows that of the entire basin.

The relative advantage of the process-oriented experiments described in this article over more sophisticated simulations (e.g., Semtner and Chervin 1992) is that because of their built-in simplifications it is relatively straightforward to associate causes and effects. The most obvious of their disadvantages is their lack of eddy resolution, particularly in the ARR, which is characterized by highly energetic eddy fields. In this regard it seems pertinent to discuss the relevance of the present results to the actual circulation and their intrinsic limitations. The argument put forward in defense of the modeling strategy was that because of the characteristics of the forcing the oceanic response was expected to consist of large-scale, mostly barotropic waves. The validity of this argument has been discussed at length in previously referenced papers (e.g., Gill and Niiler 1976; Anderson and Corry 1985) and it will not be repeated. The obvious consequence of such an assumption, however, is that the results of this model are only applicable to the large-scale circulation and its interaction with the western boundary current and not to the high-frequency dynamics of the western boundary current itself (which may include unresolved processes such as hydrodynamic instabilities or interactions with coastal regions). From this distinction it seems reasonable to expect that the conclusions on the low-frequency variability derived from our experiments will remain valid, even for eddy-resolving experiments and should be distinguishable by large-scale observations (e.g., satellite altimetry). This, indeed, seems the case. Semtner and Chervin (1992) used a high-resolution version of Bryan and Cox's model to simulate the global circulation. They calculated time series and power spectra for the transports of the Agulhas and East Madagascar Currents. For the East Madagascar Current, their Fig. 20 shows a general pattern of transport variations (for the last ten years of model simulation), which consists of a maximum during the austral summer, a decrease through the winter, and a secondary maximum during the spring. Interannual variability appears mostly limited to shifts in the exact location of the transport extremes. These high-resolution results for the East Madagascar transport are qualitatively similar to those shown in Fig. 4 ⊙ and have been identified herein as the barotropic response of the ocean to seasonally changing winds. Also, the Agulhas transport in Semtner and Chervin's simulation, unlike any other major western boundary current, shows no kind of periodicity. This is consistent with the argument put forward in this article that the buffering effect of the bottom topography in the south Indian Ocean prevents the propagation of the seasonal signal from the open ocean to the eastern margin of the African continent. In this scenario most of the Agulhas variability is related to local processes such as baroclinic and barotropic instabilities.

In spite of the numerical predictions, evidence on seasonal variations of the East Madagascar Current transport is not unambiguous. Swallow et al. (1988) and Schott et al. (1988) analyzed hydrographic and moored current meter data collected during an 11-month period in the boundary currents east of Madagascar, near 12° and 23°S, and reported that neither dataset shows a detectable seasonal cycle. A possible explanation for this lack of seasonal variation was offered by Kindle (1991), who did a series of numerical simulations using a reduced-gravity model and a two-layer model with full bottom topography. He argued that the lack of seasonal variation of the northern branch of the Madagascar Current is caused by the effect of the Mascarene Ridge and the topography asssociated with the Providence Bank. In agreement with our results, Kindle (1991) observed that the southern branch of the East Madagascar Current has significant seasonal variations and pointed out that the southernmost mooring data discussed by Schott et al. were too close to the coast to detect the predicted seasonal variations.

4. Summary and discussion

The focus of this article has been the effects of the seasonally varying winds on the southwestern Indian Ocean. Its motivation was the apparent discrepancy between in situ and remote observations on seasonal changes of the Agulhas transport. According to our numerical experiments, the portion of the Agulhas Current that flows along the eastern margin of the African continent is prevented from receiving the westward propagating signal of the seasonally varying winds by the quasi-meridional ridges that characterize the south Indian basin. This explains why hydrographic observations, mostly conducted on this portion of the flow, have been unable to detect distinct seasonal variations of the Agulhas transport (Pearce and Gründling 1982). Once the current leaves the bounding coast however, it enters a relatively large region (the ARR), which is dominated by strong, anticyclonic winds that can generate the seasonally varying anomaly patterns reported from satellite observations (Zlotnicki et al. 1989; Quartly and Srokosz 1993; Lutjeharms and van Ballegooyen 1988).

Our results indicate that there are distinct modes of variability east and west of 45°E. West of Madagascar, there is a dominant mode with a maximum during spring–summer and a minimum during fall–winter. East of Madagascar there is a marked decrease of the circulation during fall (April) and relative maximums during summer (February) and winter (August). The similarities of the time–longitude plots at 30° and 40°S (Fig. 4 ⊙) and the anomaly patterns depicted in Figs. 6 ⊙ and 9 ⊙ indicate that east of 45°E the midlatitude variability is influenced by advection and wave propagation. In the western portion of the basin, however, the damping of westward propagation from the open ocean by the quasi-meridional ridges at 45°E allows local wind forcing to create the variability in the circulation, characterized by a dominant annual mode. The conclusion from the experiments, therefore, is that although the mean transport of the Agulhas Current might be accounted for by the large-scale structure of the wind stress curl, its low-frequency variability (periods larger than a month

but less than a year) appears to be mostly determined by the effect of local winds.

According to our experiments, seasonal variations in the ARR are not related to significant changes in the upstream transport of the Agulhas Current, which are regarded as negligible, but to local interactions of the current with the wind forcing and bottom topography. The seasonal cycles derived from our experiments appear to be consistent with satellite observations, which indicate a strengthening of the circulation in the ARR during the summer and spring and a weakening during the winter. In spite of these agreements it should be noted that, since our particular model did not resolve all the dominant scales of variability, our results should be taken as a qualitative assessment of the effect of the large-scale forcing on the region. A more quantitative evaluation would require higher-resolution experiments in domains larger than those considered in this study to evaluate the interaction between the Agulhas and the Antarctic Circumpolar Current.

REFERENCES

Anderson, D. L. T., and R. A. Corry, 1985: Ocean response to low frequency forcing with application to the seasonal variations in the Florida Straits–Gulf Stream transports. *Progress in Oceanography,* Vol. 14, Pergamon, 7–40..

Boudra, D. B., and W. P. M. de Ruijter, 1986: The wind-driven circulation of the South Atlantic–Indian Ocean: II. Experiments using a multi-layer numerical model. *Deep-Sea Res.,* **33,** 447–482..

——, ,and E. P. Chassignet, 1988: Dynamics of the Agulhas retroflection and ring formation in a numerical model. Part I: The vorticity balance. *J. Phys. Oceanogr.,* **18,** 280–303.. Find this article online

Bryan, K., 1969: A numerical method for the study of the circulation of the world ocean. *J. Comput. Phys.,* **4,** 347–376..

Chassignet, E. P., and D. B. Boudra, 1988: Dynamics of Agulhas retroflection and ring formation in a numerical model. Part II: Energetics and ring formation. *J. Phys. Oceanogr.,* **18,** 304–319.. Find this article online

Cox, M. D., 1984: A primitive equation, 3-dimensional model of the ocean. GFDL Tech. Report, GFDL Ocean Group, Geophysical Fluid Dynamics Laboratory, Princeton University, Princeton, NJ..

De Ruijter, W. P. M., and D. B. Boudra, 1985: The wind-driven circulation in the South Atlantic–Indian Ocean. I: Numerical experiments in a one-layer model. *Deep-Sea Res.,* **12,** 361–373..

Ffield, A., J. Toole, and D. Wilson, 1997: Seasonal circulation in the South Indian Ocean. *Geophys. Res. Lett.,* **24,** 2773–2776..

Gill, A. E., and P. P. Niiler, 1973: The theory of seasonal variability in the ocean. *Deep-Sea Res.,* **20,** 14–47..

Gordon, A. L., 1986: Interocean exchange of thermocline waters. *J. Geophys. Res.,* **91,** 5037–5046..

Gründlingh, M. L., 1980: On the volume transport of the Agulhas Current. *Deep-Sea Res.,* **27,** 557–563..

Harris, T. F. W., 1970: Planetary-type waves in the South West Indian Ocean. *Nature,* **227,** 1043–1044..

Hellerman, S., and M. Rosenstein, 1983: Normal monthly wind stress over the world ocean with error estimates. *J. Phys. Oceanogr.,* **13,** 1093–1104.. Find this article online

Kindle, J., 1991: Topographic effects on the seasonal circulation of the Indian Ocean. *J. Geophys. Res.,* **96,** 16 827–16 837..

Lutjeharms, J. R. E., 1996: *The South Atlantic: Present and Past Circulation.* G. Wefer et al., Eds., Springer-Verlag, 125–162..

——, ,and R. C. van Ballegooyen, 1988: The retroflection of the Agulhas Current. *J. Phys. Oceanogr.,* **18,** 1570–1583.. Find this article online

Matano, R. P., 1995: Numerical experiments on the effects of a meridional ridge on the transmission of energy by barotropic Rossby waves. *J. Geophys. Res.,* **100,** 18 271–18 280..

—— ,1996: A numerical study of the Agulhas retroflection: The role of bottom topography *J. Phys. Oceanogr.,* **26,** 2267–2278.. Find this article online

Ou, H. W., and W. P. M. de Ruijter, 1986: Separation of an inertial boundary current from an irregular coastline. *J. Phys. Oceanogr.,* **16,** 280–289.. Find this article online

Pearce, A. F., and M. L. Gründlingh, 1982: Is there a seasonal variation in the Agulhas Current? *J. Mar. Res.,* **40,** 177–184..

Quartly, G. D., and M. A. Srokosz, 1993: Seasonal variations in the region of the Agulhas retroflection: Studies with Geosat and FRAM. *J. Phys. Oceanogr.,* **23,** 2107–2124.. Find this article online

Rhines, P. B., 1969: Slow oscillations in an ocean of varying depth. I: Abrupt topography. *J. Fluid Mech.,* **37,** 161–189..

Schott, F., M. Fieux, J. Kindle, J. Swallow, and R. Zantopp, 1988: The boundary currents east and north of Madagascar. 2: Direct measurements and model comparison. *J. Geophys. Res.,* **93,** 4963–4974..

Semtner, A. J., and R. M. Chervin, 1992: Ocean general circulation from a global eddy-resolving model. *J. Geophys. Res.,* **97,** 5493–5550..

Stramma, L., and J. R. E. Lutjeharms, 1997: The flow field of the subtropical gyre fo the South Indian Ocean. *J. Geophys. Res.,* **102,** 55 513–55 530..

Swallow, J., M. Fieux, and F. Schott, 1988: The boundary currents north of Madagascar. 1: Geostrophic currents and transport. *J. Geophys. Res.,* **93,** 4951–4962..

Willebrand, J. S., S. G. H. Philander, and R. C. Pacanowski, 1980: The oceanic response to large-scale atmospheric disturbances. *J. Phys. Oceanogr.,* **10,** 411–429.. Find this article online

Zlotnicki, V., L. L. Fu, and W. Patzert, 1989: Seasonal variability in global sea level observed with Geosat altimetry. *J. Geophys. Res,* **94,** 17 959–17 969..

Figures
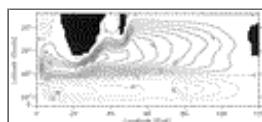

Click on thumbnail for full-sized image.

Fig. 1. Topographic features with bottom depths shallower than 3000 m in the south Indian basin.
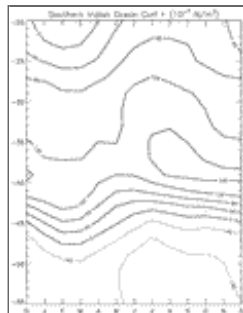
Click on thumbnail for full-sized image.

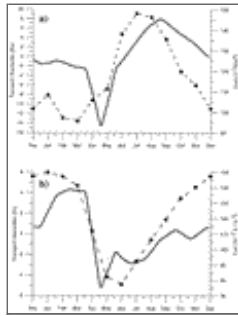Fig. 2. Seasonal variations of the zonally averaged wind stress curl in the south Indian Ocean.

Click on thumbnail for full-sized image.

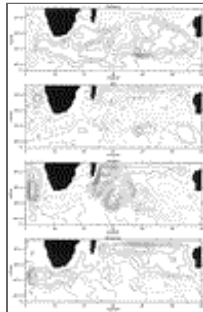Fig. 3. Annual mean distribution of the streamfunction in the baroclinic experiment. The contour interval is 5 Sv.
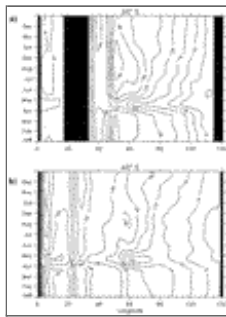
Fig. 4. Time–longitude plots of the evolution of the streamfunction in the baroclinic experiment at (a) 30°S and (b) 40°S. The solid block denotes sections covered by land.

Fig. 5. Seasonal evolution of transport anomalies (full line) and the zonally averaged wind stress curl (dotted line) at (a) 30°S and (b) 40°S.
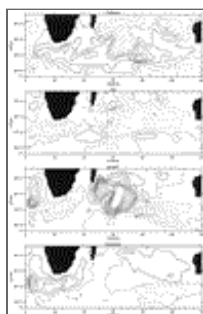
Fig. 6. Streamfunction anomalies for the baroclinic experiment. This figure was constructed by subtracting the annual mean value (Fig. 3 ⬤▬) from the monthly streamfunction distribution for February, May, August, and November. In this figure positive values (solid contours) denotes a strengthening of the circulation.
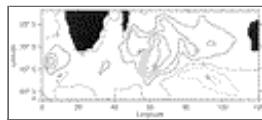
Fig. 7. Annual mean distribution of the streamfunction in the barotropic experiment. The contour interval is 5 Sv.

Fig. 8. Streamfunction anomalies for the barotropic experiment. This figure was constructed by substracting the annual mean value (Fig. 6 ⊙➥) from the monthly streamfunction distribution for February, May, August, and November. In this figure positive values (solid contours) denote a strengthening of the circulation.
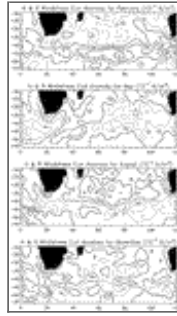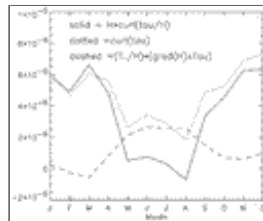

Click on thumbnail for full-sized image.

Fig. 9. Wind-stress curl anomalies for the months of February, May, August, and November. This figure was constructed by subtracting the annual mean wind stress curl distribution for the corresponding months. The wind climatology is that of Hellerman and Rosenstein (1983).
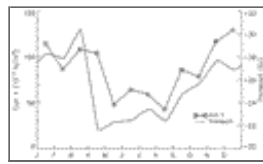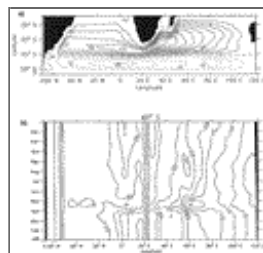

Click on thumbnail for full-sized image.

Fig. 10. Seasonal evolution of the wind stress curl averaged in the area between 35° and 45°S, 10° and 30°E and the Agulhas transport at 45°S, 20°E.

Click on thumbnail for full-sized image.

Fig. 11. Seasonal evolution of the term H^* curl(τ/H) and its components proportional to the curl of the wind (dotted line) and to the gradient of the bottom depth (dashed line).

Click on thumbnail for full-sized image.

Fig. 12. (a) Annual mean distribution of the streamfunction in an experiment conducted in an extended domain. (b) Time–longitude plot of the streamfunction evolution at 40°S.

Corresponding author address: Dr. Ricardo P. Matano, College of Oceanic and Atmospheric Sciences, Oregon State University, 104 Ocean Admin. Bldg., Corvallis, OR 97331-5503.

E-mail: rpm@oce.orst.edu